Optimized lytic polysaccharide monooxygenase action increases fiber accessibility and fibrillation by releasing tension stress in cellulose cotton fibers

Maud Chemin, Kamal Kansou, Karine Cahier, Margaux Grellier, Sacha Grisel, Bruno Novales, Celine Moreau, Ana Villares, Jean-Guy Berrin, Bernard Cathala

Optimized lytic polysaccharide monooxygenase action increases fiber accessibility and fibrillation by releasing tension stress in cellulose cotton fibers

Maud Chemin, Kamal Kansou, Karine Cahier, Margaux Grellier, Sacha Grisel, Bruno Novales, Celine Moreau, Ana Villares, Jean-Guy Berrin, Bernard Cathala*

ABSTRACT: Lytic polysaccharide monooxygenase (LPMO) enzymes have recently shaken up our knowledge on the enzymatic degradation of biopolymers and cellulose in particular. This unique class of metalloenzymes cleaves cellulose and other recalcitrant polysaccharides using an oxidative mechanism. Despite their potential in biomass saccharification and cellulose fibrillation, the detailed mode of action of LPMOs at the surface of cellulose fibers still remains poorly understood and highly challenging to investigate. In this study, we first determined the optimal parameters (temperature, pH, enzyme concentration and pulp consistency) of LPMO action on the cellulose fibers by analyzing the changes in molar mass distribution of solubilized fibers using high performance size exclusion chromatography (HPSEC). Using an experimental design approach with a fungal LPMO from the AA9 family (*Pa*LPMO9H) and cotton fibers, we revealed maximum decrease in molar mass at 26.6 ºC and pH 5.5, with 1.6% *w/w* enzyme loading in dilute cellulose dispersions (100 mg of cellulose at 0.5% *w/v*). These optimal conditions were used to further investigate the impact of *Pa*LPMO9H on the cellulosic fiber structure. Direct visualization of the fiber surface by scanning electron microscopy (SEM) revealed that *Pa*LPMO9H created cracks on the cellulose surface while attacking tension regions that triggered the rearrangement of cellulose chains. Solid-state NMR indicated that *Pa*LPMO9H increased the lateral fibril dimension and created novel accessible surfaces. This study confirms the LPMO-driven disruption of cellulose fibers and extends our knowledge on the mechanism underlying such modifications. We hypothesize that the oxidative cleavage at

the surface of the fibers releases the tension stress, with loosening of the fiber structure and peeling of the surface, thereby increasing the accessibility and facilitating fibrillation.

KEYWORDS: LPMO, response surface design, molar mass, peeling, fibrillation, cellulose nanofiber.

INTRODUCTION

Since the first report in 2010 of the monooxygenase activity and the description of the associated enzyme,[1] lytic polysaccharide monooxygenase (LPMO) enzymes have attracted much attention within the scientific community. Beyond their key role in lignocellulosic biomass degradation in nature and their addition to enzymatic cocktails for biofuels and biorefinery applications,[2, 3] they are seen as promising enzymes to reduce the energy required for cellulose fibrillation when preparing cellulose nanofibers.[4-6]

LPMOs are unique metalloenzymes containing a single type II copper ion coordinated by a solvent exposed histidine brace, allowing them to oxidize C-H bonds at the C1 and/or C4 carbon of glycosidic linkages found in recalcitrant polysaccharides such as cellulose.[7] To catalyze this challenging reaction, LPMOs control a powerful oxidative reaction that involves Fenton-like chemistry.[8] They require to be activated either by a redox enzyme partner (i.e. cellobiose dehydrogenase; CDH), small organic reductants (i.e. ascorbate, cysteine) or even lignin.[9] The nature of the co-substrate (O_2, H_2O_2) bringing the oxygen atom necessary for cleavage of the polysaccharide chain has been a matter of intensive research and debates.[10] LPMOs are distributed into eight families (AA9-AA11, AA13-AA17)[11-17] of the CAZy classification (Carbohydrate Active enZymes database; www.cazy.org).[18] The AA9 family is exclusively found in fungi, and its members are active on cellulose, cello-oligosaccharides and β-(1-4)-

linked hemicelluloses.[19-22] AA9 LPMOs can be appended to a carbohydrate-binding module (CBM) promoting binding to cellulose and activity.[23]

Traditionally, the LPMO activity on cellulosic substrates has been monitored through the detection of soluble oxidized products released after enzymatic action.[20] We first described the structural changes on the cellulose fiber resulting from LPMO activity by combining solid-state NMR and imaging techniques.[22] LPMOs create nicking points on the cellulose fiber surface, thus facilitating fiber disruption and separation.[4, 24, 25] In synergy with cellulases, LPMOs improved mechanical fibrillation of cellulose and thus facilitate nanofibrillation.[6, 26-30] Further studies have revealed the presence of oxidized groups on the cellulose fiber surface using a fluorescent probe.[31, 32] Nevertheless, evaluating LPMO action at the surface of cellulose fibers remains challenging to investigate.

In this study, we evaluated the changes in the molar mass of cellulose chains after enzymatic treatment using HPSEC coupled to an experimental design approach to identify the optimal conditions (temperature, pH, enzyme/substrate ratio and pulp consistency) of LPMO activity. Then, we investigated the LPMO action on the insoluble part of the cellulose fiber during enzymatic incubation. We also visualized modifications at the cellulose fiber surface by SEM and assessed the structural changes associated by solid-state ^{13}C NMR.

EXPERIMENTAL SECTION

Materials. Cysteine, copper sulfate, sodium acetate, acetic acid, methanol, *N*,*N*-dimethylacetamide (DMAc) and lithium chloride (LiCl) were purchased from Sigma-Aldrich. Tetrasodium (6E)-4-amino-6-[[4-[4-[N′-(8-amino-1-oxo-5,7-disulfonato-2-naphthylidene)hydrazino]-3-methoxy-phenyl]-2-methoxy-phenyl]hydrazono]-5-oxo-naphthalene-1,3-disulfonate (Direct Blue 1, DB 1) and 2,3,14,15-tetrazapentacyclo[20.2.2.24,7.210,13.216,19]dotriaconta-

1(24),2,4,6,8,10,12,14,16,18,20,22,25,27,29,31-hexadecaene-6,11,18,23-tetrasulfonic acid (Direct Orange 15, DO 15) were purchased from Pylam Dyes.

Enzyme production. The recombinant *Pa*LPMO9H from *Podospora anserina* previously expressed and characterized[20] was produced in *Pichia pastoris* in a 1 L bioreactor and purified as previously described.[16, 20]

Cellulose substrate. Cellulose from cotton was used as the cellulose substrate. Whatman paper was hydrated in water under stirring for 24 h and activated in a blender at 25 g L^{-1}. The obtained pulp was freeze-dried.

LPMO treatment. Experimental conditions for the *Pa*LPMO9H treatment (temperature, pH, enzyme/substrate ratio and pulp consistency) were determined by the experimental design (see below). Cellulose fibers (100 mg) were dispersed in acetate buffer (50 mM) adjusted at the desired pH (4-7) at a final reaction volume of 4-20 mL (pulp consistency 0.5-2.5% *w/v*). Purified *Pa*LPMO9H enzyme was added to the pulp at a final concentration of 0.1-2% *w/w* and cysteine at 48 mg g^{-1}. Enzymatic incubation was performed at 20-50 ºC under mild agitation for 0-120 h. 120 h was selected as the end point of the enzymatic reaction, even if we assume that the *Pa*LPMO9H may be deactivated before 120 h. At the end-point, *Pa*LPMO9H enzyme was deactivated by heating at 100 ºC for 10 min. Control samples consist of cellulose fibers treated at the same conditions but without *Pa*LPMO9H.

Experimental design. The exploration and the determination of the experimental conditions susceptible to favor LPMO enzymatic activity was performed using a response surface design with four factors: reaction temperature (factor a), pH (factor B), enzyme/substrate (E/S) ratio (factor C), and pulp consistency (factor D) (**Table 1**). Temperature and pH effects on the enzymatic reaction were expected to follow a second-order model, besides higher-order models were out of reach due to time and resource constraints. Temperature is a hard-to-change (HTC) factor while the other factors are easy-to-change (ETC) factors, and pulp consistency is a

categorical factor with two levels (**Table 1**). A three-factor central-composite design (CCD) within a split-plot structure[33] was created and duplicated for each pulp consistency level. Split-plot experiments involved two distinct randomizations, the randomization of the HTC factors forms the whole-plot design and, within each whole-plot section, the randomization of ETF factors forms the subplots. Usual coding for three-factors CCD is (±1, ±1, ±1) for the factorial section, (0, 0, 0) for the center point, and (±α, 0, 0), (0, ±α, 0), (0, 0, ±α) for the axial points. The value of α was chosen to accommodate all factorial and axial points on the surface of a sphere. The mapping of the factors values and coded values is supplied in **Table 1**. The design space was first framed by imposing the lowest and highest levels (i.e. ±α levels), then values corresponding to -1, 0 and +1 levels were computed according to the linear transformation.

Table 1. Mapping of the factor values and coded values for the *Pa*LPMO9H treatment of cellulose fibers.

Measurements	Factor	Levels				
		-α	**-1**	**0**	**1**	**α**
T (°C)	a	20	26.3	35	43.7	50
pH	B	4.0	4.6	5.5	6.4	7.0
E/S (% *w/w*)	C	0.1	0.5	1.1	1.6	2.0
Pulp consistency (% *w/v*)	D	-	Low (0.5)	-	High (2.5)	-

The initial plot contained a total of 42 runs, with 21 runs for each consistency level with five central points, eight factorial points, and eight axial (star) points. After a first round of experiments, the design was augmented with six additional experiments to replicate interesting points and explore further subplot axial points. The design was performed using Design-Expert® (version 12) software. Candidate response surface models were estimated via the restricted maximum likelihood approach for increasing polynomial orders (from second to fourth-order). The most informative terms of the model were selected based on the BIC

(Bayesian Information Criterion) value through backward elimination, a hierarchically well-formed polynomial was then built from the selected terms. Eventually regions of the design space with most desirable values with regard to the LPMO expected actions were identified through the built-in numerical optimization procedure of the statistical software.

High Performance Size Exclusion Chromatography (HPSEC) coupled to multi-angle laser light scattering (MALLS). Molar mass determination of cellulose chains was determined as previously described.[4] Briefly, fibers were filtered over sinter glass (porosity 16-40 µm) and then redispersed in anhydrous methanol (3×20 mL) followed by redispersion in anhydrous dimethylacetamide (3×20 mL). Then the DMAc-swollen fibers were added to 10 mL of DMAc/LiCl (9% *w/w*) under magnetic string during 3 days at 4°C before 10-fold dilution with anhydrous DMAc. The solution was then filtered (PTFE 0.45 µm) and injected on a size exclusion chromatography system (OMNISEC Resolve, Malvern) with DMAc/LiCl (0.9 % *w/v*) as the eluent. The SEC columns used were Viscotek Tguard, LT4000L, LT5000L and LT7000L. The system was equipped with a multi-angle laser light scattering Malvern SEC-MALS 20 and OMNISEC Reveal devices (Malvern). Calculations were performed with a *dn/dc* value of 0.136 mL g^{-1} and performed using OMNISEC software.

Solid-state ^{13}C CP/MAS NMR. Cellulose samples (100 mg) were rehydrated in 50 µL H_2O and water excess was absorbed using an adsorbent. About 80-100 mg of each sample was packed into the 4 mm NMR rotor. Cross-polarization magic angle (CP/MAS) NMR experiments were acquired on a Bruker Avance III 400 spectrometer operating at a ^{13}C frequency of 100.62 MHz equipped with a double resonance H/X CP/MAS 4 mm probe. Measurements were conducted at room temperature with a MAS spinning rate of 9 kHz. The CP pulse sequence parameters were: 3.5 µs proton 90° pulse, 1.75 ms CP contact time at 67.5 kHz, and 9 s recycle time. The number of acquisition for the CP/MAS ^{13}C spectra was typically 5.120 scans. ^{13}C NMR spectra were referenced to the carbonyl peak of glycine at 176.03 ppm.

All spectra were processed with Gaussian multiplication parameters of LB = -5 Hz and GB = 0.1. NMR spectra were deconvoluted using PeakFit™ (v4.12) software as previously described.[4, 22]

Polarized optical microscopy (POM). Cellulose fibers (0.1 g L^{-1} in milliQ water) were deposited onto a glass slide, dried at 40°C, and observed by a BX51 polarizing microscope (Olympus France S.A.S.) with a 4× objective. Images were captured by a U-CMAD3 camera displaying a U-TV0.5XC-3 adaptor (Olympus Japan). Twisting counting was performed on 20 images containing at least 30 individual cellulose fibers.

Simons' staining. Cellulose fibrillation was observed using Simons' staining. The stain consists in a 1% *w/v* aqueous solution of Direct Blue 1 and a 1% *w/v* aqueous solution of Direct Orange 15 mixed in a 1:1 ratio. Untreated and enzyme-treated fibers (10 mg) were soaked in 60 µL of stain solution overnight. The fibers were then washed with milliQ water and filtered (PC 5 µm) before redispersion in milliQ water. A drop of the dispersion was deposited onto a glass slide, dried at 40°C, and observed by a BX51 polarizing microscope (Olympus France S.A.S.) with a 4× objective.

Scanning electron microscopy (SEM). Cellulose fibers (0.1 g L^{-1} in milliQ water) were deposited onto an adhesive carbon pad, dried at 40°C and observed with a Quattro scanning electron microscope at low-vacuum (Thermo Scientific).

RESULTS AND DISCUSSION

Optimal conditions of *Pa*LPMO9H activity evaluated by HPSEC. Cotton linters were chosen as the cellulose model substrate because they consist of almost pure cellulose (only 3% of hemicelluloses)[34] with rather high chain length, being a representative cellulosic substrate. We selected an AA9 LPMO from *Podospora anserina* (*Pa*LPMO9H), which contains a CBM1 and preferentially catalyzes C4 oxidative cleavage of cellulose.[20] We studied the impact of four

parameters (temperature, pH, enzyme/substrate ratio and pulp consistency) on its activity on cotton cellulose fibers. The range of temperature was from 20 to 50 ºC, and the pH was studied from 4 to 7. The enzyme/substrate ratio was investigated from 0.1 to 2.0% *w/w*, and we investigated two pulp consistencies, 0.5 and 2.5% *w/v*. An experimental design of a total of 42 runs was produced (Table S1). The *Pa*LPMO9H activity was monitored as the changes in the molar mass distribution. For this purpose, the cellulose fibers were solubilized in DMAc/LiCl and analyzed by high performance size exclusion chromatography (HPSEC). HPSEC data allowed the calculation of average weight molar mass (M_w), the average number molar mass (M_n) and the polydispersity index (M_w/M_n), which represented the response variables in the experimental plan. Table S1 shows the experimental design conditions and the results from HPSEC.

A model selection procedure was used to generate and assess quadratic, cubic and quartic models with all combinations of terms, called full model, and with a selection of terms that represented the best compromise between the number of factors and the fitting performances, called reduced model. The modelling performances were assessed the best trade-off between the maximization of adjusted R^2 (Adj. R^2) and the minimization of Akaike Information Criterion (AIC), both widely used for model selection. Results of the model selection procedure are reported in **Figure 1**.

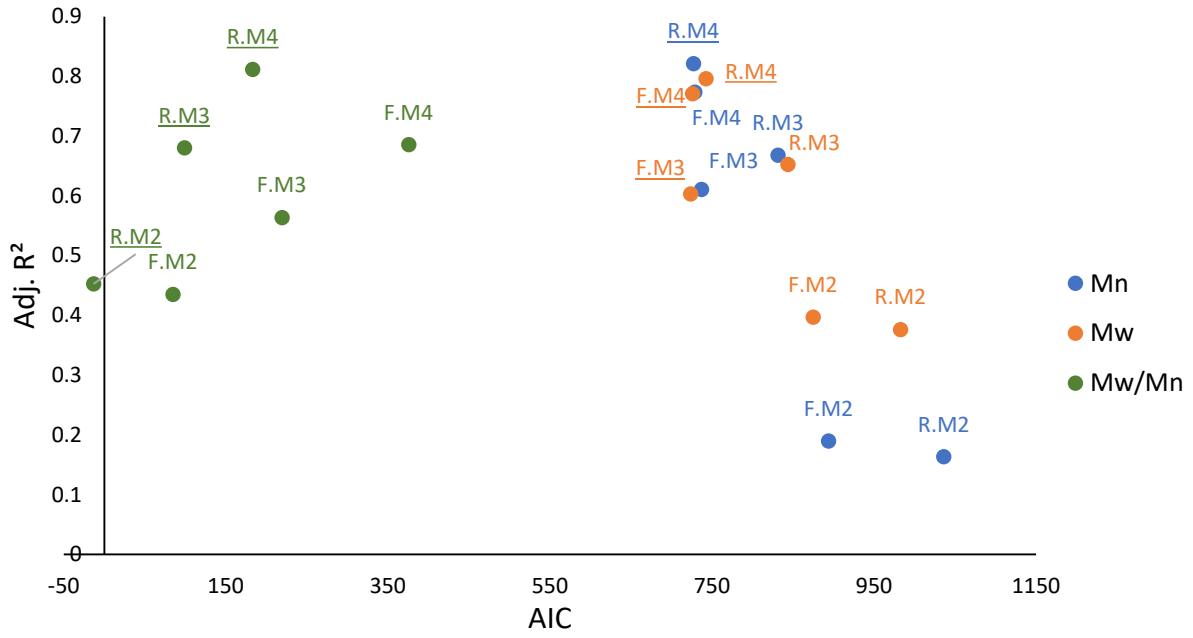

Figure 1. Results of the model selection procedure for Adj.R² and AIC. Dominant solutions, i.e. best for Adj.R² or for AIC, are underlined. F.M*i* stands for Full Model of polynomial degree *i*, R.M*i* stands for Reduced Model of polynomial degree *i*.

The three response variables were all poorly fitted by the quadratic models, as shown by the low values of Adj.R² obtained for F.M2 and R.M2 in **Figure 1**. The reduced quartic models (R.M4) were dominant solutions, for M_n, M_w and M_w/M_n. In the case of M_n, R.M4 was the unique dominant solution, i.e. best for Adj.R² and for AIC. For illustration this model is supplied in Figure S1 and Table S2. While the reduced quartic models present in general the best performances, the experimental plan should ideally be augmented to reach robust parameterization of such high-order models. They can nevertheless be used to frame a design space most likely to favor the *Pa*LPMO9H activity – the desirable area – using a built-in numerical analysis provided by Design Expert® software. The constraints and preferences used for the numerical analysis are supplied in Table S3.

The desirable area for *Pa*LPMO9H activity lies within the following boundaries:

26 °C < Temperature < 30 °C

5 < pH < 5.7

E/S ratio = upper range value

Pulp consistency = Low

Notice that the outcomes of the numerical analysis were essentially driven by the results for M_n (and in turn by M_w/M_n) which was more responsive to *Pa*LPMO9H activity than M_w in the conditions of the experimental design.

The selected conditions of the *Pa*LPMO9H activity within the desirable area were a temperature of 26.6 ºC, pH 5.5, 1.6% *w/w* of *Pa*LPMO9H enzyme, and pulp consistency of 0.5% *w/v*. This meets only partially the conditions used in most of the studies of LPMO activity on cellulose, performed at pH 5-6 and at 50 ºC.[11, 12, 20, 31, 35-38] The desirable area was consistent with the pH range, however it did not support the positive effect of high temperatures on LPMO activity. In many cases reported in the literature, the reaction conditions were chosen for practical reasons, i.e. to be compatible with the cellulases (endoglucanases, cellobiohydrolases) used concomitantly with LPMO enzymes for the saccharification of lignocellulosic biomass. Nevertheless, the optimal temperature in our experimental set up was around 26 ºC, consistent with the natural environment of the coprophilous fungus *Podospora anserina*.

Regarding the E/S ratio and pulp consistency, there are wide ranges of LPMO and pulp concentrations used in literature.[26, 29-31, 36-39] When LPMO activity is evaluated in rather amorphous and well-dispersed systems, such as phosphoric acid swollen cellulose (PASC) or regenerated amorphous cellulose (RAC), the enzyme/substrate ratio ranges from 0.5 to 5% *w/w* and the pulp consistency is lower than 0.5% *w/v*.[31, 37, 38] When insoluble cellulosic substrates are used, the E/S ratio ranges from 0.1 to >10% *w/w* and pulp consistency can be increased to 20-25% *w/v*.[26, 29, 30, 36] This pulp concentration is typically encountered during pulp manufacturing and Kraft pulp processing.[39] In previous studies, we have evaluated the impact of enzyme concentration (0.1-2% *w/w*) on the fibrillation of cellulose fibers.[22] Our results

showed a greater disrupting effect for higher *Pa*LPMO9H concentrations (2% *w/w*). In this study, we demonstrate that the *Pa*LPMO9H activity was optimal at 1.6% *w/w*, which means an overall reduction compared to enzyme loading used in literature (9-12% *w/w*).[29] Moreover, our work revealed that lower fiber consistency (0.5% *w/v*) favored the *Pa*LPMO9H activity, which was in agreement with previous studies on pulp treatments by enzymatic cocktails. In this field, Hu et al.[40] observed that increasing pulp consistency significantly decreased the activity of cellulases even if reinforced with xylanase and LPMO enzymes. When the pulp consistency increased from 10 to 20% *w/v*, the enzyme concentration required to achieve the same degree of hydrolysis was almost three times higher.

Changes in molar mass with time during *Pa*LPMO9H action. We next examined the time course of *Pa*LPMO9H activity at the optimal conditions. HPSEC studies allowed us to obtain the average weight molar mass distributions at different reaction times. We selected a wide time range (up to 120 h) to better characterize the enzymatic end-point. The analysis of MALLS responses permitted to calculate the changes in M_w, M_n, the degree of polymerization (DP_w), and M_w/M_n, as a function of time (Table 2).

Table 2. Weight average molar mass (M_w), number average molar mass (M_n), degree of polymerization (DP_w), polydispersity (M_w/M_n) and recovery range of cellulose cotton fibers after *Pa*LPMOH treatment at different times (control, 24 h and end-point). Results are expressed as mean ± standard deviation.

	M_w (10^3 g mol^{-1})	M_n (10^3 g mol^{-1})	DP_w	M_w/M_n	Recovery (%)
Control	302±6	227±5	1865±36	1.3±0.0	75-107
24 h	289±29	184±21	1784±177	1.6±0.1	65-99
End-point	258±11	175±5	1592±67	1.5±0.0	102-103

Furthermore, distribution of molar masses gave us more insight into the kinetics of the LPMO reaction. Figure 2 shows molar mass distribution of cotton fibers for control, at 24 h and at the end-point of the enzymatic treatments. One has to note that all recovery yields calculated from elution peak, i.e. after dissolution and chromatographic analysis, were higher than 75% (Table 2); therefore, the results were significant. The molar mass distribution of starting cellulose chains displayed a narrow and symmetrical distribution with rather low polydispersity of 1.3, and M_w and M_n of about 302 × 10^3 and 258 × 10^3 g mol^{-1} (Table 2). During the first 24 h *Pa*LPMO9H action, the molar mass distribution profile changed little. As the enzymatic reaction time increased from 24 h to the end-point, there was an appreciable shift towards lower molar masses and an increase in the low molar mass fraction, and both M_w and M_n decreased significantly and in a larger extend than the standard deviation of the measurement, leading to the conclusion that *Pa*LPMO9H has clearly the ability to cleave the cellulose chains (Table 2).

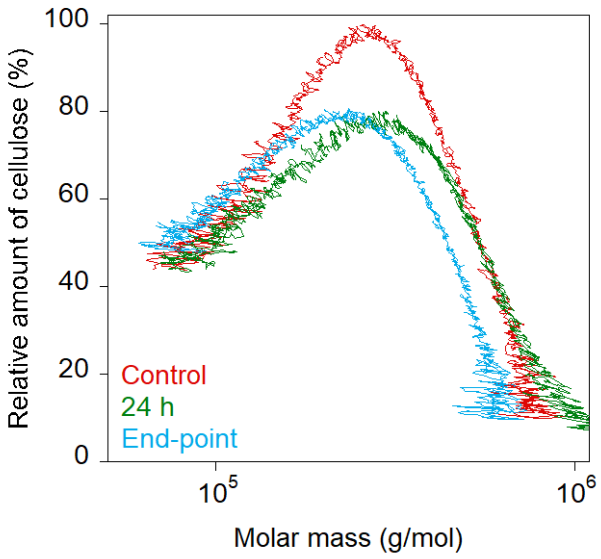

Figure 2. Molar mass distribution profiles of *Pa*LPMO9H-treated cotton fibers. Normalized molar mass distribution profiles of cellulose cotton fibers after *Pa*LPMO9H treatment: control, at 24 h and at end-point.

Moreover, after 24 h of enzymatic action, the polydispersity reflected by the M_w/M_n ratio increased, suggesting the formation of low molecular weight chains that broadened the distribution. However, the DP of the neo-formed chains remained high as they remained insoluble in water and can be detected by MALLS. At the same time, the recovery yield remained stable (and even increased slightly), indicating that no soluble sugars were released. Indeed, if soluble sugars were formed by the *Pa*LPMO9H action, they would be removed during the solvent exchange step of the cellulose solubilization procedure in DMAc/LiCl, leading to a decrease of recovery yield. Previous works have shown that the action of the LPMO on the cellulose fibers produces little or no soluble products.[22, 23] *Pa*LPMO9H induced a reduction in the molar mass of the cellulose; however, these changes were very subtle, which suggested that the *Pa*LPMO9H action could be restricted to a limited and/or specific region of the cellulose chains. At the nanoscale, the surface chains represent about 20-25% of the total chains, but as the fiber size increases, the proportion of surface chains decreases drastically. At the end-point of *Pa*LPMO9H action, the cellulose chains degradation was more pronounced since M_w and M_n decreased of 15 and 22% respectively (Table 2). The M_w/M_n ratio had a value close to that of 24 h degradation (end-point 1.5 and 24 h 1.6) and higher than at the starting point (1.3). It has also to be noted that the recovery yield, which reflects the cellulose dissolution, increased remarkably and was almost quantitative, suggesting that *Pa*LPMO9H facilitated the dissolution and thus the solvent penetration into the fibers. This point is consistent with the fibrillation and swelling action of LPMOs previously demonstrated.[4]

The action of the cellulose-degrading enzymes on the molar mass distribution can be schematically viewed as two modes of action: cleavage from the end (exo-action) or random cleavage along the polymer chains (endo-action).[41-43] In the first case, the DP should decrease slowly as well as the polydispersity while in the second scenario, molar mass is expected to decrease rapidly while polydispersity increases.[44-46] In the case of *Pa*LPMO9H, the molar mass

decreases slowly and the polydispersity increases. Two assumptions can be proposed. The first one takes into account the structure of the fibers. Since the surface chains are less abundant than the bulk ones, *Pa*LPMO9H may act preferentially at the surface by creating low molar mass chains and increasing polydispersity, but the majority of the chains being in the bulk of the fibers, the molar mass decreases slightly. The second hypothesis is that the *Pa*LPMO9H might act on specific regions of the fibers resulting in targeted fiber degradation leading to the generation of low molar mass fragments while the majority of the chains remains unchanged. However, a combination of factors, i.e. attack of specific zones at the surface of the fiber, cannot be ruled out. Therefore, SEM and NMR investigations have been conducted to investigate more precisely the mechanism of action of this LPMO.

Structural changes associated to *Pa*LPMO9H action on the cellulose fiber. We evaluated the impact of *Pa*LPMO9H action of the cellulose cotton fiber morphology by optical and electronic microscopy. Microscopy images showed tangible differences in fiber morphology upon *Pa*LPMO9H action (**Figure 3**). Polarized optical microscopy (POM) (**Figure 3**a-c) allowed to visualize the whole fiber, and the images showed that *Pa*LPMO9H triggered the dissociation of the fiber into microfibrils at certain regions, and this effect was more pronounced as the reaction time increased. Figure S2 shows more POM and scanning electron microscopy (SEM) images illustrating *Pa*LPMO9H action. In contrast to previous studies,[4, 22, 29] microfibrils remained linked to the cellulose fiber as no mechanical treatment was applied after the enzymatic reaction. The red arrows in **Figure 3**a-c indicate the fiber twisting. Tension or tensional regions correspond to internal fiber stresses that induce mechanical deformation of the fibers, i.e. fiber twist. This can be due to biosynthetic reasons (adhesion of the middle lamellar, maturation stress in the tension wood...) or to treatmens applied to the fibers (anisotropic drying, shear, etc...).[47-49] By image analysis over 20 POM images for each sample, containing at least 50 fibers, we counted the number of twists per number of fibers. Without

*Pa*LPMO9H treatment, 44% of cellulose fibers were twisted while at the end-point, the percentage of twisted fibers was reduced to 36%.

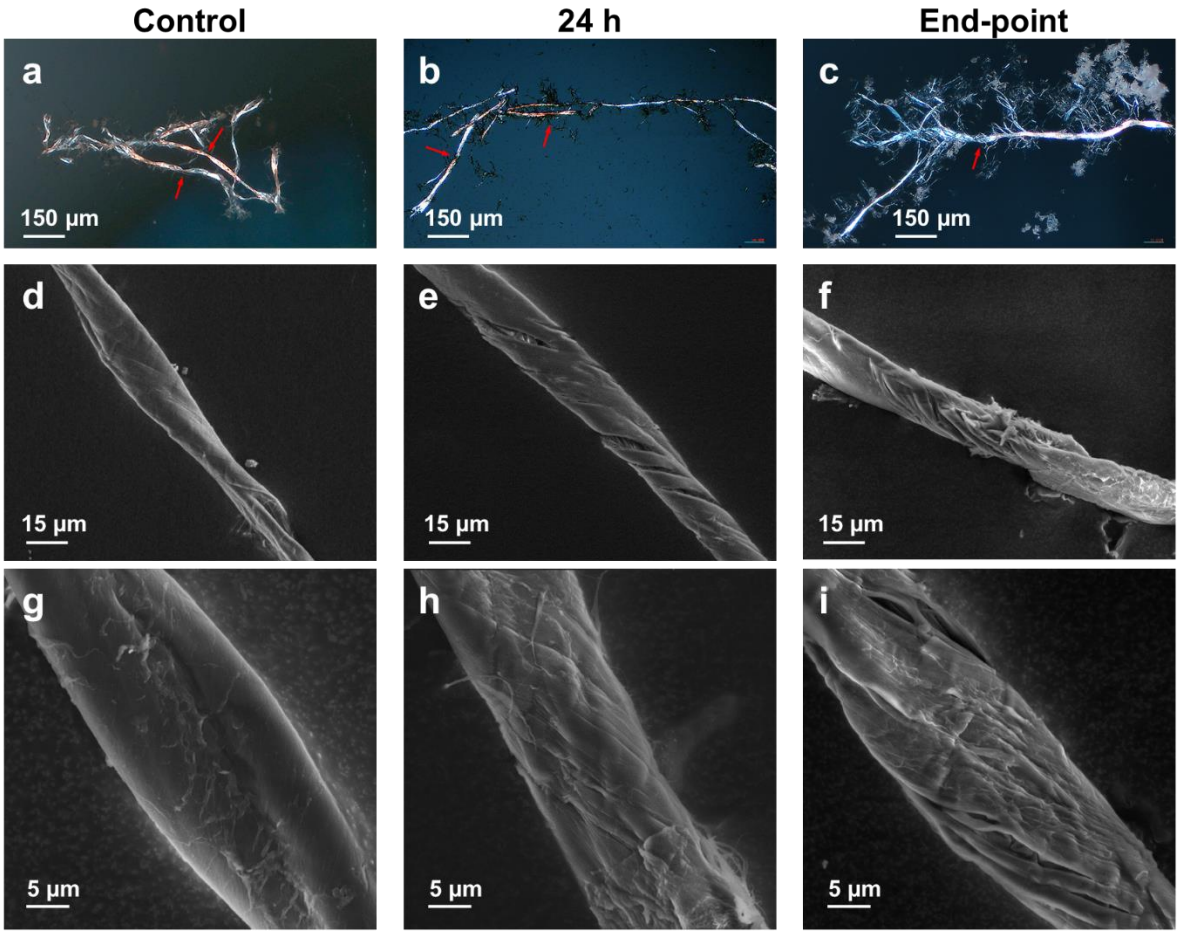

Figure 3. Morphology of LPMO-treated cellulose. Polarized optical microscopy images (top, a-c) and scanning electronic microscopy (SEM) images (bottom, d-i) of cellulose cotton fibers after *Pa*LPMO9H treatment at different times (control, 24 h and end-point).

SEM allowed visualizing morphological changes on the fiber surface (**Figure 3**d-i). Control fibers showed a rather smooth surface. They appeared to be ribbon-like and occasionally fibers turn along the long axis, presenting some twists (**Figure 3**d and g). Upon incubation for 24 h, surface roughness increased as *Pa*LPMO9H seemed to create a particular pattern of cracks and wrinkles in the outer layer of the fiber surface (**Figure 3**e and h). Then, at the end-point, the specific arrangement of the fiber seemed disrupted, as the cracks became deeper and fibril

aggregates were separated and, in some cases, disintegrated (**Figure 3**f and i). Upon *Pa*LPMO9H action, the appearance of cracks seemed to release the tension within the fiber because some dislocations were removed. This result could indicate that *Pa*LPMO9H attacks these specific tensional regions of the fibers. Therefore, *Pa*LPMO9H releases the tightness, and therefore, increases the fiber accessibility and facilitates fibrillation. Then, according to the molar mass reduction and the disappearance of high molar mass fractions observed by HPSEC, *Pa*LPMO9H could continue attacking by digging into the fiber among different chains, with its subsequent loosening.

To demonstrate the higher accessibility of cellulose fibers after LPMO action, we performed Simons' staining on control and *Pa*LPMO9H-treated samples. Simons' staining is a differential staining comprised of two different stains of different molecular weights. Direct Blue 1 (DB 1) has a low molecular weight around 992.82 10^3 g mol^{-1} while Direct Orange 15 (DO 15) is a polymeric mixture containing a high molecular weight fraction (above 25 000 10^3 g mol^{-1}).[50] During the staining, the DB 1 dye first penetrates the cellulose fiber's pores, thanks to its small particle size. When the fiber is treated with the enzyme, the fibrillation leads to an increase in the pores size, which allows the DO 15 dye to penetrate the pores, as the affinity of DO 15 for cellulose is more important than the affinity of DB 1.[50]

On the control (**Figure 4**), the majority of fibers was dyed with DB 1 because the fibers have not been treated with the enzyme. However, the fibers were still subjected to a light mechanical treatment (stirring for 48 h) that could impact the fiber integrity. This phenomenon can explain the presence of fibers dyed in orange in the control. In the condition treated with the enzyme (24 h and end-point), an increase of the fibers dyed with DO 15 could be observed. This tendency was more evident as the reaction time increased, which confirmed that the *Pa*LPMO9H facilitated the fibrillation. This method allowed for a more visual observation of

the fibrillation but it is still not precise enough to evaluate quantitatively the impact of the enzyme on the cellulose fibers.

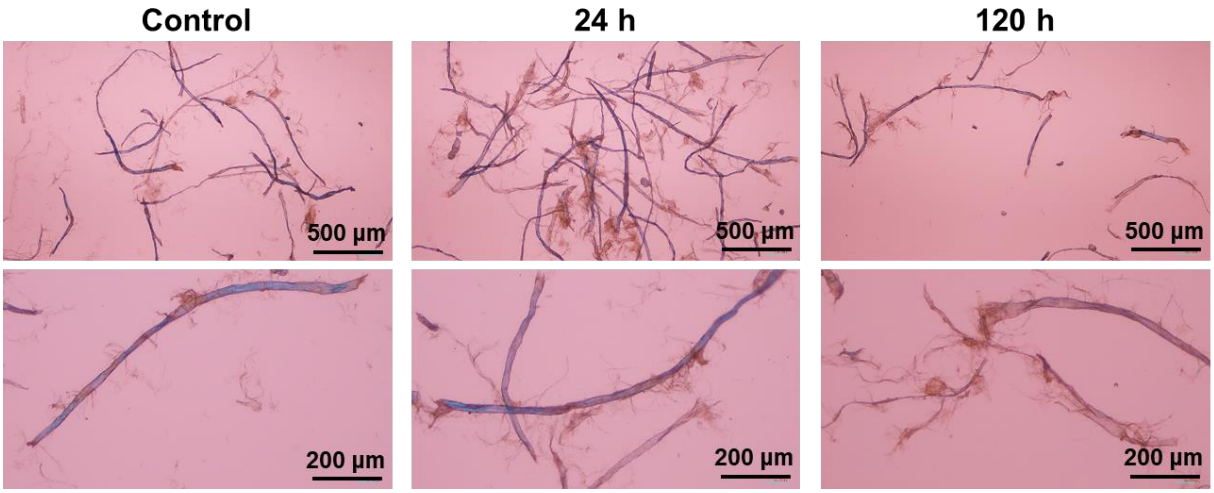

Figure 4. Direct visualization by optical microscopy of Simons' staining of cellulose cotton fibers images previously treated with *Pa*LPMO9H at different times (0, 24 h and end-point).

Solid-state ^{13}C CP/MAS NMR spectra were recorded on cellulose cotton fibers upon *Pa*LPMO9H action for control, 24 h and at the end-point (**Figure 5**). Spectra showed the distinct signals typical of cellulose carbons with C1 (δ 102-106 ppm), C4 (δ 78-89 ppm), C2,3,5 (δ 70-76 ppm) and C6 (δ 55-69 ppm). Deconvolution of NMR spectra, and in particular peaks from the C4 region, was performed based on our previous works[4, 14, 22] and on Larsson work[34] (**Figure 5**, right).

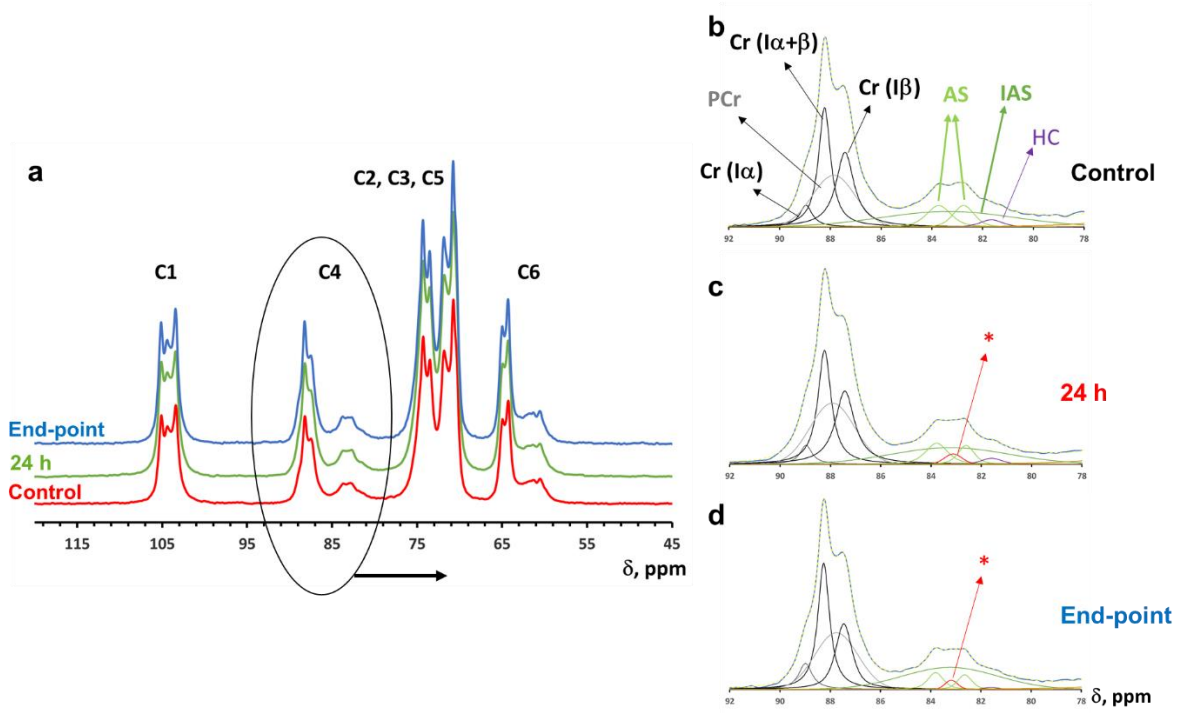

Figure 5. a Solid-state ^{13}C CP/MAS NMR spectra of cotton fibers after *Pa*LPMO9H treatment: control, 24 h and end-point (left). b-d Deconvolution of the corresponding C4 regions with crystalline forms Cr(I_α), Cr(I_β) and Cr($I_{\alpha+\beta}$) (black), para-crystalline form (PCr) (grey), accessible fibril surfaces (AS) (green), and inaccessible fibril surface (IAS) (dark green) signals for the cotton fibers treated with *Pa*LPMO9H: control (b), 24 h (c) and end-point (d). HC peak (purple) refers to carbon signal from residual hemicellulose. For *Pa*LPMO9H-treated samples, an additional peak is denoted by (*, red) (see text for details).

As shown in the spectrum of control fibers, C4 crystalline region corresponded to three sharp signals from Cr(I_α) at 89.0 ppm, Cr(I_α+I_β) at 88.2 ppm and Cr(I_β) at 87.4 ppm, and the paracrystalline (PCr) at 87.9 ppm. In the amorphous C4 region, two peaks at 83.8 and 82.7 ppm corresponding to carbons on the accessible surfaces (AS) of cellulose are superimposed to a very broad signal centered at 83.3 ppm, which are C4 carbons located on inaccessible surfaces (IAS). The peak at around 81.5 ppm was assigned to residual hemicelluloses (HC), such as

xylan.[4, 34] The relative contribution of each peak from the C4 deconvolution are listed in Table S4.

The *Pa*LPMO9H action (at 24 h and beyond) resulted in the appearance of a small additional signal at 83.2 ppm (denoted as * in red in **Figure 5**). This signal displayed a narrow width (~260 Hz) as compared to other signals, which indicated higher molecular mobility. The peak area significantly increased with enzyme reaction time (from 0.9 to 1.8%), which confirmed that the signal was due to the *Pa*LPMO9H action. As previously described,[22] the occurrence of this small peak was attributed to amorphous cellulose chains released by the *Pa*LPMO9H treatment and accessible to the surrounding solvent. This feature was thus consistent with HPSEC results and microscopy investigations that suggested higher solvent accessibility after *Pa*LPMO9H action.

At the same time, hemicelluloses content (HC signal at 81.5 ppm) decreased significantly during the course of *Pa*LPMO9H treatment. It represented 2.8±0.3% for the control, in agreement with Larsson et al.[34] who found 3.1±1.6% hemicelluloses (xylan) from the deconvolution of the C4 region of the cotton cellulose spectrum. After *Pa*LPMO9H treatment, HC content decreased significantly to about 1% (Table S4) allowing to formulate two hypotheses: (i) some of the hemicelluloses were removed from cellulose surface chains due to *Pa*LPMO9H action, or (ii) cellulose chains on which hemicelluloses were adsorbed underwent a profound change thus modifying the environment of the hemicelluloses.

From the peak deconvolution, several structural information on cellulose fibers were obtained (**Table 3**). The degree of crystallinity (CrI) did not significantly change upon *Pa*LPMO9H action (from 69.5±2.2% for the control, to 71.7±1.4% after *Pa*LPMOH treatment) regardless of the duration of the *Pa*LPMOH action. Nevertheless, the proportion of accessible carbons in the amorphous part (AS/(AS+IAS)) strongly decreased beyond 24h-LPMO action (from ~31.6 to 19.6) confirming that *Pa*LPMOH acts on accessible surfaces of cellulose fibrils creating

specific nicking points that probably lead to chain breaking at the fiber surface. This fact also supported the hypothesis that hemicellulose loss would be associated with the decrease of signal from cellulose accessible surfaces. In this context, the occurrence of the new small peak (*) observed in LPMO-treated spectra (**Figure 5**) could be assigned to chains with higher mobility released by the enzyme action.

Table 3. Values of crystallinity, accessible/total fibril surface ratio (AS/(AS+IAS)), lateral fibril dimensions (LFD) and lateral fibril aggregate dimensions (LFAD) calculated from the C-4 region deconvolution of the solid-state ^{13}C CP/MAS NMR spectra of control and *Pa*LPMOH-treated cellulose samples. Results are expressed as mean (standard deviation).

Sample	CrI (%)	AS/(AS+IAS)	LFD (nm)	LFAD (nm)
Control	69.5 *(2.2)*	31.6 *(1.0)*	6.9 (*0.5*)	24.0 (*5.6*)
24 h	71.5 *(1.6)*	31.2 *(0.6)*	7.4 (*0.4*)	24.9 (*2.0*)
End-point	71.7 *(1.4)*	19.6 *(0.7)*	7.4 (*0.3*)	39.5 (*0.8*)

The lateral fibril dimensions (LFD) and lateral fibril aggregate dimensions (LFAD) were estimated from the C4 peak deconvolution considering a square cross-sectional cellulose microfibril model and a conversion factor of 0.57 width.[51-53] LFD of cellulose fibers was 6.9±0.5 nm, which was in agreement with values reported for cotton linters[54] and other cellulosic substrates.[55] During *Pa*LPMO9H action, fibril dimensions did not significantly change (7.4±0.4 nm at 24 h and at end-point). Differently, LFAD remained constant for the first 24 h (from 24.0±5.6 for control to 24.9±2.0 nm at 24 h) and then dramatically increased to 39.5±0.8 nm at the end-point. This increase in LFAD (from about 24 nm to 39 nm) in

*Pa*LPMO9H-treated cellulose fibers confirmed our previous results explained by the aggregation and swelling of fibrils after enzymatic action.[22] According to the SEM images, the increase in LFAD could also be associated to the removal of tension zones in the fiber. The release of such tightly associated dislocations would therefore create more swollen and accessible arrangements, which facilitate the fibrillation by mechanical treatments, as we have previously described.[4]

Overall, our results indicate that *P*aLPMO9H seems to attack specific sites on the cellulose surface. SEM images showed that tension regions (twists) were disrupted upon *P*aLPMO9H action, and therefore, the release of tightly associated dislocations could create swollen and more accessible surfaces (**Figure 6**).

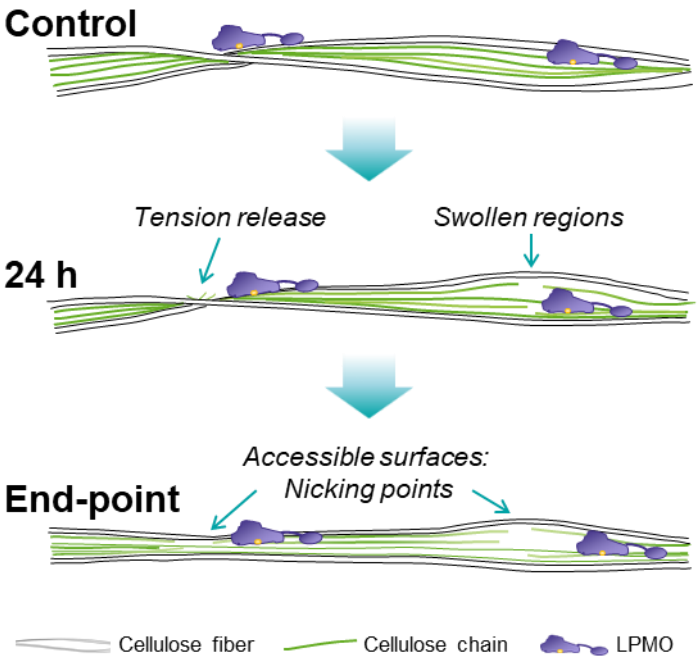

Figure 6. Schematic representation of the *P*aLPMO9H mechanism of action on the cotton cellulose fiber. Cellulose chains are represented as green lines. Elements (fiber, cellulose chains and the LPMO enzyme) are not scaled.

In cotton fibers, the presence of twists has been associated to the desiccation occurring at the end of the fiber growth.[47] Singh et al.[48] postulated that the cotton fiber may twist to consolidate

the fiber bundles, and this organization would allow the fiber elongation in a confined space (the locule), and would act as a junction layer in the middle lamella. The LPMO action on cell joint regions would explain its key role and boosting activity in degrading lignocellulose biomass,[56] but further studies are necessary to investigate if LPMOs would specifically attack adhesion zones in plant cell wall.

CONCLUSION

In this study, we have investigated the mechanism of action of the *Pa*LPMO9H enzyme on insoluble cellulose substrates. HPSEC results pointed at a random scission *Pa*LPMO9H mode of action on the cotton fibers leading to the decrease of molar mass and polydispersity increase in a first step. This finding is consistent with *P*aLPMO9H action on the fiber surface and, possibly in targeted areas. *Pa*LPMO9H could therefore adsorb on the cellulose surface, cleave the chains by the oxidative mechanism and render the fiber looser and solvated, increasing the cellulose chains accessibility as demonstrated by solubilization yields, strong fibrillation and higher proportion of surface chains in NMR. From the SEM images, *Pa*LPMO9H seems to attack the cellulose surface, more precisely the regions where cellulose chains display some tension. Therefore, *Pa*LPMO9H action would result in partial relaxation of fibril distortions, leading to additional degrees of freedom in the cellulose chain organization. This would result in the formation of a new type of accessible surface, as the new NMR signal at 83.2 ppm suggested.[22] Then, the association of several fibrils would result in the significant LFAD increase observed at the end-point of the enzymatic reaction.

ASSOCIATED CONTENT

Supporting information

AUTHOR INFORMATION

Corresponding Author

Bernard Cathala − UR1268 BIA, INRAE, F-44316 Nantes, France; orcid.org/0000-0002-3844-872X;

Email: bernard.cathala@inrae.fr

Authors

Maud Chemin − UR1268 BIA, INRAE, F-44316 Nantes, France

Kamal Kansou − UR1268 BIA, INRAE, F-44316 Nantes, France

Karine Cahier − UR1268 BIA, INRAE, F-44316 Nantes, France

Margaux Grellier − UR1268 BIA, INRAE, F-44316 Nantes, France

Sacha Grisel – INRAE, Aix Marseille Univ., UMR BBF, F-13009 Marseille, France ; INRAE, Aix Marseille Univ., 3PE platform, F-13009 Marseille, France ; orcid.org/0000-0001-6983-0107

Bruno Novales – INRAE, BIBS facility, PROBE infrastructure, F-44316 Nantes, France

Celine Moreau − UR1268 BIA, INRAE, F-44316 Nantes, France

Ana Villares − UR1268 BIA, INRAE, F-44316 Nantes, France; orcid.org/0000-0001-5441-7299

Jean-Guy Berrin – INRAE, Aix Marseille Univ., UMR BBF, F-13009 Marseille, France ; orcid.org/0000-0001-7570-3745 ; INRAE, Aix Marseille Univ., 3PE platform, F-13009 Marseille, France ; orcid.org/0000-0001-7570-3745

Author Contributions

Conceptualization, B.C. and J.G.B.; funding acquisition, J.G.B.; investigation, M.C., K.K., K.C., M.G., S.G., B.N. and C.M.; project administration, A.V.; writing – original draft, A.V.; writing – review and editing, M.C., K.K., K.C., M.G., S.G., B.N., C.M., J.G.B. and B.C.

Notes

The authors declare no competing financial interest.

ACKNOWLEDGEMENTS

The authors gratefully acknowledge the 3BCar Carnot Institute for financial support (Fonzy project). The authors acknowledge the BIBS platform of INRAE for the access to NMR (Xavier Falourd) and microscopy facilities.

REFERENCES

(1) Vaaje-Kolstad, G.; Westereng, B.; Horn, S. J.; Liu, Z.; Zhai, H.; Sorlie, M.; Eijsink, V. G. H. An Oxidative Enzyme Boosting the Enzymatic Conversion of Recalcitrant Polysaccharides. *Science* **2010**, *330* (6001), 219-222.
(2) Johansen, K. S. Discovery and industrial applications of lytic polysaccharide mono-oxygenases. *Biochem Soc Trans* **2016**, *44* (1), 143-149.
(3) Muller, G.; Varnai, A.; Johansen, K. S.; Eijsink, V. G. H.; Horn, S. J. Harnessing the potential of LPMO-containing cellulase cocktails poses new demands on processing conditions. *Biotechnol. Biofuels* **2015**, *8*.
(4) Moreau, C.; Tapin-Lingua, S.; Grisel, S.; Gimbert, I.; Le Gall, S.; Meyer, V.; Petit-Conil, M.; Berrin, J. G.; Cathala, B.; Villares, A. Lytic polysaccharide monooxygenases (LPMOs) facilitate cellulose nanofibrils production. *Biotechnol. Biofuels* **2019**, *12*.
(5) Karnaouri, A.; Chorozian, K.; Zouraris, D.; Karantonis, A.; Topakas, E.; Rova, U.; Christakopoulos, P. Lytic polysaccharide monooxygenases as powerful tools in enzymatically assisted preparation of nano-scaled cellulose from lignocellulose: A review. *Bioresour Technol* **2022**, *345*, 126491.
(6) Valenzuela, S. V.; Valls, C.; Schink, V.; Sánchez, D.; Roncero, M. B.; Diaz, P.; Martínez, J.; Pastor, F. I. J. Differential activity of lytic polysaccharide monooxygenases on celluloses of different crystallinity. Effectiveness in the sustainable production of cellulose nanofibrils. *Carbohydr. Polym.* **2019**, *207*, 59-67.
(7) Tandrup, T.; Frandsen, K. E. H.; Johansen, K. S.; Berrin, J.-G.; Lo Leggio, L. Recent insights into lytic polysaccharide monooxygenases (LPMOs). *Biochem. Soc. Trans.* **2018**, *46*, 1431-1447.
(8) Bissaro, B.; Eijsink, V. G. H. Lytic polysaccharide monooxygenases: enzymes for controlled and site-specific Fenton-like chemistry. *Essays in biochemistry* **2023**.
(9) Hemsworth, Glyn R. Revisiting the role of electron donors in lytic polysaccharide monooxygenase biochemistry. *Essays in biochemistry* **2023**, *67* (3), 585-595.
(10) Vandhana, T. M.; Reyre, J. L.; Sushmaa, D.; Berrin, J. G.; Bissaro, B.; Madhuprakash, J. On the expansion of biological functions of lytic polysaccharide monooxygenases. *The New phytologist* **2022**, *233* (6), 2380-2396.
(11) Isaksen, T.; Westereng, B.; Aachmann, F. L.; Agger, J. W.; Kracher, D.; Kittl, R.; Ludwig, R.; Haltrich, D.; Eijsink, V. G. H.; Horn, S. J. A C4-oxidizing Lytic Polysaccharide Monooxygenase Cleaving Both Cellulose and Cello-oligosaccharides. *Journal of Biological Chemistry* **2014**, *289* (5), 2632-2642.

(12) Forsberg, Z.; Mackenzie, A. K.; Sorlie, M.; Rohr, A. K.; Helland, R.; Arvai, A. S.; Vaaje-Kolstad, G.; Eijsink, V. G. H. Structural and functional characterization of a conserved pair of bacterial cellulose-oxidizing lytic polysaccharide monooxygenases. *Proceedings of the National Academy of Sciences of the United States of America* **2014**, *111* (23), 8446-8451.
(13) Hemsworth, G. R.; Henrissat, B.; Davies, G. J.; Walton, P. H. Discovery and characterization of a new family of lytic polysaccharide rnonooxygenases. *Nat. Chem. Biol.* **2014**, *10* (2), 122-126.
(14) Couturier, M.; Ladeveze, S.; Sulzenbacher, G.; Ciano, L.; Fanuel, M.; Moreau, C.; Villares, A.; Cathala, B.; Chaspoul, F.; Frandsen, K. E.; et al. Lytic xylan oxidases from wood-decay fungi unlock biomass degradation. *Nat. Chem. Biol.* **2018**, *14* (3), 306-+.
(15) Sabbadin, F.; Hemsworth, G. R.; Ciano, L.; Henrissat, B.; Dupree, P.; Tryfona, T.; Marques, R. D. S.; Sweeney, S. T.; Besser, K.; Elias, L.; et al. An ancient family of lytic polysaccharide monooxygenases with roles in arthropod development and biomass digestion. *Nat. Commun.* **2018**, *9*.
(16) Filiatrault-Chastel, C.; Navarro, D.; Haon, M.; Grisel, S.; Herpoël-Gimbert, I.; Chevret, D.; Fanuel, M.; Henrissat, B.; Heiss-Blanquet, S.; Margeot, A.; et al. AA16, a new lytic polysaccharide monooxygenase family identified in fungal secretomes. *Biotechnol. Biofuels* **2019**, *12* (1), 55.
(17) Sabbadin, F.; Urresti, S.; Henrissat, B.; Avrova, A. O.; Welsh, L. R. J.; Lindley, P. J.; Csukai, M.; Squires, J. N.; Walton, P. H.; Davies, G. J.; et al. Secreted pectin monooxygenases drive plant infection by pathogenic oomycetes. *Science* **2021**, *373* (6556), 774-779.
(18) Drula, E.; Garron, M. L.; Dogan, S.; Lombard, V.; Henrissat, B.; Terrapon, N. The carbohydrate-active enzyme database: functions and literature. *Nucleic acids research* **2022**, *50* (D1), D571-D577.
(19) Vu, V. V.; Beeson, W. T.; Phillips, C. M.; Cate, J. H. D.; Marletta, M. A. Determinants of Regioselective Hydroxylation in the Fungal Polysaccharide Monooxygenases. *J. Am. Chem. Soc.* **2014**, *136* (2), 562-565.
(20) Bennati-Granier, C.; Garajova, S.; Champion, C.; Grisel, S.; Haon, M.; Zhou, S.; Fanuel, M.; Ropartz, D.; Rogniaux, H.; Gimbert, I.; et al. Substrate specificity and regioselectivity of fungal AA9 lytic polysaccharide monooxygenases secreted by *Podospora anserina*. *Biotechnol. Biofuels* **2015**, *8*, 90.
(21) Fanuel, M.; Garajova, S.; Ropartz, D.; McGregor, N.; Brumer, H.; Rogniaux, H.; Berrin, J. G. The *Podospora anserina* lytic polysaccharide monooxygenase PaLPMO9H catalyzes oxidative cleavage of diverse plant cell wall matrix glycans. *Biotechnol. Biofuels* **2017**, *10*.
(22) Villares, A.; Moreau, C.; Bennati-Granier, C.; Garajova, S.; Foucat, L.; Falourd, X.; Saake, B.; Berrin, J. G.; Cathala, B. Lytic polysaccharide monooxygenases disrupt the cellulose fibers structure. *Sci Rep* **2017**, *7*, 40262.
(23) Chalak, A.; Villares, A.; Moreau, C.; Haon, M.; Grisel, S.; d'Orlando, A.; Herpoel-Gimbert, I.; Labourel, A.; Cathala, B.; Berrin, J. G. Influence of the carbohydrate-binding module on the activity of a fungal AA9 lytic polysaccharide monooxygenase on cellulosic substrates. *Biotechnol. Biofuels* **2019**, *12* (1), 206.
(24) Ladeveze, S.; Haon, M.; Villares, A.; Cathala, B.; Grisel, S.; Herpoel-Gimbert, I.; Henrissat, B.; Berrin, J. G. The yeast Geotrichum candidum encodes functional lytic polysaccharide monooxygenases. *Biotechnol. Biofuels* **2017**, *10*, 215.
(25) Karnaouri, A.; Chorozian, K.; Zouraris, D.; Karantonis, A.; Topakas, E.; Rova, U.; Christakopoulos, P. Lytic polysaccharide monooxygenases as powerful tools in enzymatically assisted preparation of nano-scaled cellulose from lignocellulose: A review. *Bioresour. Technol.* **2022**, *345*, 126491.

(26) Valls, C.; Pastor, F. I. J.; Roncero, M. B.; Vidal, T.; Diaz, P.; Martinez, J.; Valenzuela, S. V. Assessing the enzymatic effects of cellulases and LPMO in improving mechanical fibrillation of cotton linters. *Biotechnol. Biofuels* **2019**, *12*.
(27) Han, X. S.; Bi, R.; Khatri, V.; Oguzlu, H.; Takada, M.; Jiang, J. G.; Jiang, F.; Bao, J.; Saddler, J. N. Use of Endoglucanase and Accessory Enzymes to Facilitate Mechanical Pulp Nanofibrillation. *Acs Sustainable Chemistry & Engineering* **2021**, *9* (3), 1406-1413.
(28) Rossi, B. R.; Pellegrini, V. O. A.; Cortez, A. A.; Chiromito, E. M. S.; Carvalho, A. J. F.; Pinto, L. O.; Rezende, C. A.; Mastelaro, V. R.; Polikarpov, I. Cellulose nanofibers production using a set of recombinant enzymes. *Carbohydr. Polym.* **2021**, *256*, 117510.
(29) Koskela, S.; Wang, S.; Xu, D.; Yang, X.; Li, K.; Berglund, L. A.; McKee, L. S.; Bulone, V.; Zhou, Q. Lytic polysaccharide monooxygenase (LPMO) mediated production of ultra-fine cellulose nanofibres from delignified softwood fibres. *Green Chem.* **2019**, *21* (21), 5924-5933.
(30) Hu, J.; Tian, D.; Renneckar, S.; Saddler, J. N. Enzyme mediated nanofibrillation of cellulose by the synergistic actions of an endoglucanase, lytic polysaccharide monooxygenase (LPMO) and xylanase. *Sci Rep* **2018**, *8* (1), 3195.
(31) Eibinger, M.; Ganner, T.; Bubner, P.; Rosker, S.; Kracher, D.; Haltrich, D.; Ludwig, R.; Plank, H.; Nidetzky, B. Cellulose Surface Degradation by a Lytic Polysaccharide Monooxygenase and Its Effect on Cellulase Hydrolytic Efficiency. *Journal of Biological Chemistry* **2014**, *289* (52), 35929-35938.
(32) Uchiyama, T.; Uchihashi, T.; Ishida, T.; Nakamura, A.; Vermaas, J. V.; Crowley, M. F.; Samejima, M.; Beckham, G. T.; Igarashi, K. Lytic polysaccharide monooxygenase increases cellobiohydrolases activity by promoting decrystallization of cellulose surface. *Science Advances* **2022**, *8* (51), eade5155.
(33) Vining, G. G.; Kowalski, S. M.; Montgomery, D. C. Response surface designs within a split-plot structure. *Journal of Quality Technology* **2005**, *37* (2), 115-129.
(34) Larsson, P. T.; Wickholm, K.; Iversen, T. A CP/MAS C-13 NMR investigation of molecular ordering in celluloses. *Carbohydr. Res.* **1997**, *302* (1-2), 19-25.
(35) Quinlan, R. J.; Sweeney, M. D.; Lo Leggio, L.; Otten, H.; Poulsen, J.-C. N.; Johansen, K. S.; Krogh, K. B. R. M.; Jorgensen, C. I.; Tovborg, M.; Anthonsen, A.; et al. Insights into the oxidative degradation of cellulose by a copper metalloenzyme that exploits biomass components. *Proceedings of the National Academy of Sciences of the United States of America* **2011**, *108* (37), 15079-15084.
(36) Cannella, D.; Hsieh, C. C.; Felby, C.; Jorgensen, H. Production and effect of aldonic acids during enzymatic hydrolysis of lignocellulose at high dry matter content. *Biotechnol. Biofuels* **2012**, *5* (26), (30 April 2012)-(2030 April 2012).
(37) Bey, M.; Zhou, S.; Poidevin, L.; Henrissat, B.; Coutinho, P. M.; Berrin, J.-G.; Sigoillot, J.-C. Cello-Oligosaccharide Oxidation Reveals Differences between Two Lytic Polysaccharide Monooxygenases (Family GH61) from *Podospora anserina*. *Appl. Environ. Microbiol.* **2013**, *79* (2), 488-496.
(38) Frommhagen, M.; Sforza, S.; Westphal, A. H.; Visser, J.; Hinz, S. W. A.; Koetsier, M. J.; van Berkel, W. J. H.; Gruppen, H.; Kabel, M. A. Discovery of the combined oxidative cleavage of plant xylan and cellulose by a new fungal polysaccharide monooxygenase. *Biotechnol. Biofuels* **2015**, *8*.
(39) Zhang, X.; Qin, W.; Paice, M. G.; Saddler, J. N. High consistency enzymatic hydrolysis of hardwood substrates. *Bioresour. Technol.* **2009**, *100* (23), 5890-5897.
(40) Hu, J.; Chandra, R.; Arantes, V.; Gourlay, K.; van Dyk, J. S.; Saddler, J. N. The addition of accessory enzymes enhances the hydrolytic performance of cellulase enzymes at high solid loadings. *Bioresour. Technol.* **2015**, *186*, 149-153.
(41) Jeoh, T.; Cardona, M. J.; Karuna, N.; Mudinoor, A. R.; Nill, J. Mechanistic kinetic models of enzymatic cellulose hydrolysis—A review. *Biotechnol. Bioeng.* **2017**, *114* (7), 1369-1385.

(42) Arantes, V.; Saddler, J. N. Access to cellulose limits the efficiency of enzymatic hydrolysis: the role of amorphogenesis. *Biotechnol. Biofuels* **2010**, *3*.
(43) Zhang, Y.-H. P.; Lynd, L. R. Toward an aggregated understanding of enzymatic hydrolysis of cellulose: Noncomplexed cellulase systems. *Biotechnol. Bioeng.* **2004**, *88* (7), 797-824.
(44) Zhang, M. J.; Su, R. X.; Qi, W.; Du, R. Y.; He, Z. M. Enzymatic Hydrolysis of Cellulose with Different Crystallinities Studied by Means of SEC-MALLS. *Chinese Journal of Chemical Engineering* **2011**, *19* (5), 773-778.
(45) Srisodsuk, M.; Kleman-Leyer, K.; Keranen, S.; Kirk, T. K.; Teeri, T. T. Modes of action on cotton and bacterial cellulose of a homologous endoglucanase-exoglucanase pair from Trichoderma reesei. *European Journal of Biochemistry* **1998**, *251* (3), 885-892.
(46) Stålbrand, H.; Mansfield, S. D.; Saddler, J. N.; Kilburn, D. G.; Warren, R. A.; Gilkes, N. R. Analysis of molecular size distributions of cellulose molecules during hydrolysis of cellulose by recombinant Cellulomonas fimi beta-1,4-glucanases. *Appl Environ Microbiol* **1998**, *64* (7), 2374-2379.
(47) Le Moigne, N.; Bikard, J.; Navard, P. Rotation and contraction of native and regenerated cellulose fibers upon swelling and dissolution: the role of morphological and stress unbalances. *Cellulose* **2010**, *17* (3), 507-519.
(48) Singh, B.; Avci, U.; Eichler Inwood, S. E.; Grimson, M. J.; Landgraf, J.; Mohnen, D.; Sørensen, I.; Wilkerson, C. G.; Willats, W. G. T.; Haigler, C. H. A Specialized Outer Layer of the Primary Cell Wall Joins Elongating Cotton Fibers into Tissue-Like Bundles *Plant Physiology* **2009**, *150* (2), 684-699.
(49) Clair, B.; Alméras, T.; Yamamoto, H.; Okuyama, T.; Sugiyama, J. Mechanical Behavior of Cellulose Microfibrils in Tension Wood, in Relation with Maturation Stress Generation. *Biophysical Journal* **2006**, *91* (3), 1128-1135.
(50) Fernando, D.; Daniel, G. Characterization of spruce thermomechanical pulps at the fiber cell wall level: a method for quantitatively assessing pulp fiber development using Simons' stain. *Tappi Journal* **2010**, *9* (10), 47-55.
(51) Newman, R. H. Evidence for assignment of C-13 NMR signals to cellulose crystallite surfaces in wood, pulp and isolated celluloses. *Holzforschung* **1998**, *52* (2), 157-159.
(52) Wickholm, K.; Larsson, P. T.; Iversen, T. Assignment of non-crystalline forms in cellulose I by CP/MAS C-13 NMR spectroscopy. *Carbohydr. Res.* **1998**, *312* (3), 123-129.
(53) Zuckerstätter, G.; Schild, G.; Wollboldt, P.; Röder, T.; Weber, H. K.; Sixta, H. The elucidation of cellulose supramolecular structure by ^{13}C CP-MAS NMR. *Lenzinger Berichte* **2009**, *87*, 38-46.
(54) Malm, E.; Bulone, V.; Wickholm, K.; Larsson, P. T.; Iversen, T. The surface structure of well-ordered native cellulose fibrils in contact with water. *Carbohydr. Res.* **2010**, *345* (1), 97-100.
(55) Peciulyte, A.; Karlstoem, K.; Larsson, P. T.; Olsson, L. Impact of the supramolecular structure of cellulose on the efficiency of enzymatic hydrolysis. *Biotechnol. Biofuels* **2015**, *8*, 56.
(56) Tokin, R.; Ipsen, J. O.; Westh, P.; Johansen, K. S. The synergy between LPMOs and cellulases in enzymatic saccharification of cellulose is both enzyme- and substrate-dependent. *Biotechnol. Lett.* **2020**, *42* (10), 1975-1984.